Mutations associated with familial Parkinson's disease alter the initiation and amplification steps of α-synuclein aggregation

Patrick Flagmeier[a], Georg Meisl[a], Michele Vendruscolo[a], Tuomas P. J. Knowles[a], Christopher M. Dobson[a,1], Alexander K. Buell[a,1,2], and Céline Galvagnion[a,1]

[a]Department of Chemistry, University of Cambridge, Cambridge CB2 1EW, United Kingdom

Edited by Gregory A. Petsko, Weill Cornell Medical College, New York, NY,and approved July 19, 2016 (received for review March 21, 2016)

Parkinson's disease is a highly debilitating neurodegenerative condition whose pathological hallmark is the presence in nerve cells of proteinacious deposits, known as Lewy bodies, composed primarily of amyloid fibrils of α-synuclein. Several missense mutations in the gene encoding α-synuclein have been associated with familial variants of Parkinson's disease and have been shown to affect the kinetics of the aggregation of the protein. Using a combination of experimental and theoretical approaches, we present a systematic in vitro study of the influence of disease-associated single-point mutations on the individual processes involved in α-synuclein aggregation into amyloid fibrils. We find that lipid-induced fibril production and surface catalyzed fibril amplification are the processes most strongly affected by these mutations and show that familial mutations can induce dramatic changes in the crucial processes thought to be associated with the initiation and spreading of the aggregation of α-synuclein.

lipid-induced aggregation | seeded aggregation | kinetic analysis | familial Parkinson's disease | neurodegenerative disease

The protein α-synuclein is expressed abundantly in the brain [representing up to 1% of all proteins in the neuronal cytosol (1)], especially in dopaminergic neurons, where it has been suggested to interact with the membranes of synaptic vesicles containing dopamine (2–7). During their life cycle in dopaminergic neurons, synaptic vesicles undergo variations in pH ranging from 7.4, during the process of fusion with the plasma membrane, to 5.5, during storage as a resting pool of vesicles and when the vesicles are being loaded with neurotransmitters (8–11). Furthermore, α-synuclein has been suggested to be degraded via lysosomal pathways which can have pH values as low as 5.5 (12). These examples indicate that the local pH environment experienced by α-synuclein can change very significantly during its functional cycle. α-Synuclein has also been identified as the major constituent of Lewy bodies, intraneuronal inclusions found in the brains of patients suffering from Parkinson's disease and a number of related neurodegenerative disorders including dementia with Lewy bodies (13). In addition, studies of families with a history of Parkinson's disease have resulted in the identification of a series of familial mutations (Fig. 1), leading to early-onset (A30P, E46K, A53T, G51D) or late-onset (H50Q) forms of the disease (14–19). Large variations in the age of disease onset have, however, been observed in each case (Fig. 1) (19).

The effects of these sequence changes on the kinetics of the overall aggregation of α-synuclein have been the subject of intense studies since the discovery of this protein as the main constituent of Lewy bodies (13, 22–31). The A53T variant is generally considered to accelerate aggregation compared with the WT protein (22), but less agreement exists concerning the effects of the A30P mutation, because this variant has been variously reported to aggregate more slowly (28), more rapidly (23–26), or with the same rate (22) as the WT protein. Moreover, for the E46K (27) and H50Q (29, 30) variants, the aggregation process has been reported to be accelerated compared with WT α-synuclein, but the G51D variant has been reported to aggregate more slowly than the WT protein (31). These studies provide key insights into the influence of the mutations on the overall aggregation process, but a more detailed knowledge of how the individual microscopic processes of the aggregation reaction are affected by each of the disease-associated, single-point mutations would be of considerable additional value (32–34) (Fig. 1).

A distinctive feature of the process of amyloid formation by α-synuclein, as indicated by in vitro studies, is that homogeneous primary nucleation (i.e., the formation of growth-competent nuclei directly from monomeric species in bulk solution) is undetectably slow (20). It is well established, however, that the nucleation process is strongly enhanced in the presence of surfaces, such as those of lipid vesicles (21, 35) or hydrophobic polymers [in the form of nanoparticles (36) or macroscopic surfaces (37)]. In the case of lipid membranes, the chemical properties of the lipids composing the membrane were shown to influence very significantly the magnitude by which they can trigger the aggregation of α-synuclein, suggesting a role of the membrane composition in balancing normal and aberrant behavior of the protein (38). In addition, although aggregation is not normally observed under quiescent conditions in the absence of appropriate surfaces, the addition of preformed seed fibrils allows the growth of aggregates

Significance

Proteinaceous deposits composed primarily of amyloid fibrils of α-synuclein are a hallmark of a range of neurological disorders including Parkinson's disease. Mutations of the gene encoding α-synuclein have been associated with familial variants of Parkinson's disease and lead to early- and late-onset forms of the disease. Using a combination of experimental and theoretical approaches specifically designed for the study of α-synuclein, we report that the mutations dramatically affect the rate of lipid-induced fibril production and surface-catalyzed fibril amplification processes. Such a systematic study provides new insights into the influence that single-amino acid replacements in α-synuclein can have on the two steps of α-synuclein aggregation that are likely to be crucial for disease: the initial formation of aggregates and their proliferation.

Author contributions: P.F., C.M.D., A.K.B., and C.G. designed research; P.F. and C.G. performed research; P.F., G.M., M.V., T.P.J.K., C.M.D., A.K.B., and C.G. analyzed data; and P.F., G.M., M.V., T.P.J.K., C.M.D., A.K.B., and C.G. wrote the paper.

The authors declare no conflict of interest.

This article is a PNAS Direct Submission.

Freely available online through the PNAS open access option.

[1]To whom correspondence may be addressed. Email: cmd44@cam.ac.uk, alexander.buell@uni-duesseldorf.de, or cg393@cam.ac.uk.

[2]Present address: Institute of Physical Biology, University of Düsseldorf, 40225 Düsseldorf, Germany.

This article contains supporting information online at www.pnas.org/lookup/suppl/doi:10.1073/pnas.1604645113/-/DCSupplemental.

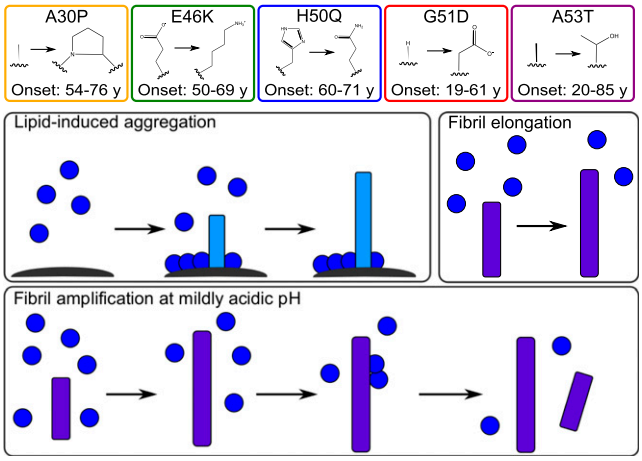

Fig. 1. Disease-associated mutations of α-synuclein and specific steps in the mechanism of aggregation. (*Upper*) Schematic illustration of the mutational variants of α-synuclein associated with familial Parkinson's disease. The amino acid substitution and the range of the age of onset reported in patients are indicated in each case (19). (*Lower*) Schematic summary of individual processes involved in the aggregation of WT α-synuclein (20, 21).

to be studied under well-defined conditions (20, 39). Indeed, if experiments are carried out at low concentrations of seed fibrils, secondary processes, by which existing fibrils amplify in number, can be directly studied. In this context, it has recently been found that the aggregation mechanism of α-synuclein is highly dependent on the solution conditions, in particular the pH of the solution (20). The quantities of added seed fibrils and the pH of the solution can, therefore, be used to adjust the relative contributions of the growth and proliferation of α-synuclein fibrils.

On the basis of this progress in our understanding of the complex mechanism of α-synuclein aggregation, we have developed and used a strategy in which individual microscopic processes in the overall aggregation reaction are probed by experiments under specifically designed conditions. To study the initial formation of fibrils from soluble monomeric species, we investigated lipid-induced aggregation by adding lipid vesicles to solutions of monomeric α-synuclein at neutral pH (21). The growth of fibrils was separately studied by addition of high (micromolar) concentrations of preformed fibrils to solutions of monomeric α-synuclein at neutral pH (20). Finally, we studied fibril amplification through secondary nucleation, by adding low (nanomolar) concentrations of preformed fibrils to solutions of monomeric α-synuclein under mildly acidic pH conditions (20, 37). Such a three-pronged strategy is particularly well suited for the study of aggregation and fibril formation by α-synuclein, because it considerably simplifies the mechanistic analysis of kinetic data, reflects the fact that the protein is exposed to varying environmental conditions during its cellular life cycle (2–7, 40, 41) and allows the study of the effect of each point mutation on each of the microscopic steps of α-synuclein aggregation.

Our results reveal that the rate of fibril elongation is only affected to a small extent by the changes in the amino acid sequence of α-synuclein associated with familial Parkinson's disease. However, we find that these mutations can alter by several orders of magnitude the rates of the initiation of fibril production induced by lipid vesicles and of their proliferation through autocatalysis at the surfaces of existing fibrils and hence dramatically change the relative importance of specific steps within the mechanism of amyloid fibril formation.

Results

The Rate of Lipid-Induced α-Synuclein Aggregation Is Dramatically Altered by the Mutations. The first set of experiments was carried out in the presence of negatively charged lipid vesicles, conditions we have recently reported to increase the rate of primary nucleation of α-synuclein amyloid formation by several orders of magnitude (21). First, we used CD to monitor the transition from the highly disordered solution state to the α-helical membrane bound state of the mutational variants associated with the binding to vesicles prepared from 1,2-dimyristoyl-sn-glycero-3-phospho-L-serine (DMPS) (21) and to determine their binding affinity to these vesicles, as described previously for WT α-synuclein (21) (*SI Appendix*, Fig. S1 *A* and *B*). All of the lipid-binding curves are well described by a one-step binding model (21), and both the WT and mutant forms of α-synuclein bind to the vesicles in conformations with high degrees of α-helicity and with submicromolar affinity (*SI Appendix*, Fig. S1*A*). Interestingly, the number of lipid molecules associated with each molecule of α-synuclein, determined from these fits, is very similar for WT (28.2 ± 0.8), A30P (33.2 ± 3.4), E46K (30.4 ± 1.6), H50Q (35.2 ± 2.1), and A53T (26.7 ± 1.1) (within experimental error; *SI Appendix*, Fig. S1) but is notably higher for G51D (42.5 ± 4.5) (see *SI Appendix* for more details). This observation, together with the fact that the lipid-bound G51D shows a smaller degree of α-helicity (less than 70% of that of WT), is consistent with the expectation that a smaller region of each G51D molecule is associated with the membrane surface in a compact helical state and that a larger region of G51D is unfolded and therefore could generate greater steric hindrance than that of WT at the surface of the vesicles. In addition, binding of each of the α-synuclein variants to DMPS vesicles induces a reduction in the melting temperature of the constituent lipids (*SI Appendix*, Fig. S1*C*), as previously observed for WT α-synuclein (21), indicating a higher binding affinity of the WT protein and the mutational variants studied here for the membrane in its fluid phase rather than in its gel phase (38).

Having characterized the binding of the proteins to the lipid vesicles, we monitored the kinetics of amyloid formation by the mutational variants in the presence of DMPS vesicles (Fig. 2 and *SI Appendix*, Fig. S2). The aggregation rate of A30P was slightly enhanced (Fig. 2*B*) and that of A53T was markedly enhanced (Fig. 2*F*) compared with that of the WT protein (Fig. 2*A*), whereas the rates of H50Q (Fig. 2*D*), E46K (Fig. 2*C*), and G51D (Fig. 2*E*) were much slower than that of WT. The fibrils formed by A30P and A53T in the presence of the DMPS vesicles were found to have a morphology very similar to that of the fibrils formed by WT α-synuclein under these conditions; in all these cases, thin fibrillar structures characteristic of protofilaments [2.6 ± 0.4 nm (WT), 3.4 ± 0.6 nm (A30P), and 2.9 ± 0.7 nm (A53T) in diameter] attached to small spherical species (attributable to the vesicles) were the dominant species visible in the AFM images (Fig. 2 *A*, *B*, and *F*, *Insets*). It is interesting in this context that the amino acid substitution in the familial Parkinson's disease-associated variants of α-synuclein are all within the region containing residues 26–97, which have been reported to modulate the interaction and affinity of the protein to membranes (42) (Fig. 2*G*). Interestingly, in the case of H50Q, a second aggregation phase was observed at longer times (~70 h) under quiescent conditions, which is characterized by the formation of fibrils with a morphology similar to that of the mature fibrils formed by WT α-synuclein under conditions where the nucleation reaction takes place at air–water or water–polymer interfaces (6.6 ± 0.9 nm in diameter; *SI Appendix*, Fig. S2*B*) (20). The intensity of the thioflavin-T (ThT) fluorescence of the H50Q fibrillar sample at the end of the second phase was observed to be an order of magnitude higher than that of the first phase and indeed of that of the other variants (i.e., WT, A30P, E46K, and A53T) (Fig. 2 and *SI Appendix*, Fig. S2*B*) under these conditions, indicating that ThT binds differently to the mature fibrils than to lipid-induced protofilaments.

In the light of these observation, we then analyzed the aggregation kinetics in detail using a one-step nucleation model (21), in which the nucleation reaction is assumed to occur at the

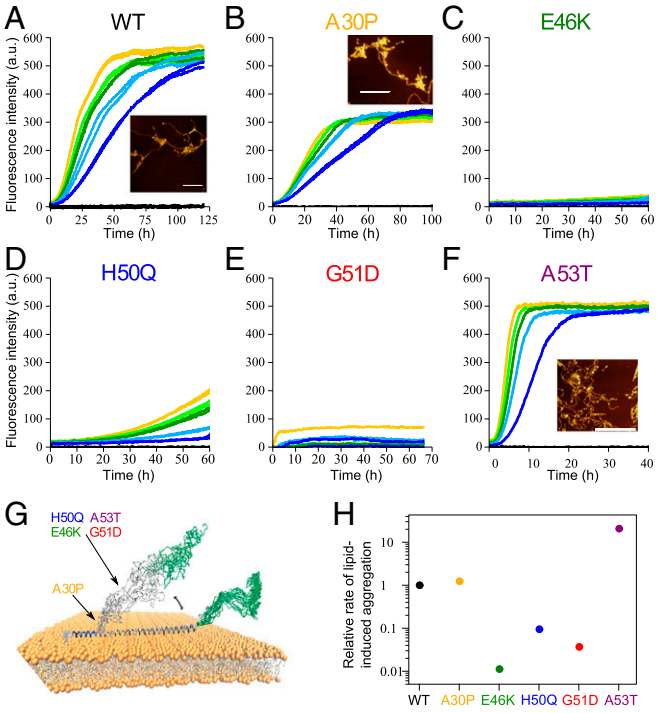

Fig. 2. The rate of lipid-induced α-synuclein aggregation is dramatically altered by the disease-related mutations. (*A*–*F*) Change in ThT fluorescence intensity when monomeric α-synuclein [WT (*A*), A30P (*B*), E46K (*C*), H50Q (*D*), G51D (*E*), and A53T (*F*)] was incubated in the absence (black) and in the presence of 100 μM DMPS under quiescent conditions at pH 6.5 and 30 °C. The protein concentrations used in this study were: 20 μM (dark blue), 40 μM (light blue), 60 μM (green), 80 μM (light green), and 100 μM (yellow). The *Insets* in *A*, *B*, and *F* show the AFM images of the fibrils formed under these conditions. (Scale bars: 1 μm.) a.u., arbitrary units. (*G*) Schematic illustration of α-synuclein interacting with a lipid bilayer highlighting the positions of the mutations in the membrane sensor region which has been reported to modulate the membrane binding affinity. Adapted from ref. 42 with permission from Macmillan Publishers Ltd: *Nature Communications*, copyright (2014). (*H*) Relative rate of lipid-induced α-synuclein aggregation, determined by fitting the early times of the aggregation curves of each mutant to a one-step nucleation model (*SI Appendix*, Fig. S3).

surface of the vesicles and is then followed by the growth of fibrils from the vesicle-bound nuclei (Fig. 2*H* and *SI Appendix*, Fig. S3). Our global analysis shows that the A30P mutation does not notably affect the lipid-induced aggregation rate, whereas the A53T mutation increases this rate by approximately two orders of magnitude relative to that of WT α-synuclein. The mutations E46K, H50Q, and G51D all decrease the lipid-induced aggregation rate, by one (H50Q) or two (E46K, G51D) orders of magnitude, relative to that of WT α-synuclein (Fig. 2*H*).

α-Synuclein Fibril Elongation at Neutral pH Is Only Weakly Influenced by the Mutations. We next carried out experiments that involved measurements of the aggregation kinetics of WT α-synuclein and variants (A30P, E46K, H50Q, G51D, and A53T) in the presence of 5 μM preformed seed fibrils (monomer equivalent concentration) at pH 6.5 under quiescent conditions, where the kinetics are dominated by elongation of the added seeds (20). We observed that the monomeric forms of all of the sequence variants of α-synuclein were able to elongate the preformed fibrils of all variants (Fig. 3*A* and *SI Appendix*, Fig. S4). To facilitate direct comparison of the variants, in each case, the measured elongation rates were normalized relative to that of "homogeneous" elongation (i.e., to the elongation rate of fibrils of a given variant by monomeric protein molecules of the same variant). We found that in all cases, such normalized elongation rates varied by less than one order of magnitude, except for the value determined for monomeric G51D, which elongates the fibrils of different variants notably more slowly (Fig. 3*B*). Interestingly, the variants in which the amino acid substitution is situated within the region known to form the β-sheet rich core of the fibrils (i.e., E46K, H50Q, G51D, and A53T) were found to have the highest rates of elongation when the monomers elongated their own seed fibrils (i.e., for homogeneous elongation) (Fig. 3*B*). The morphologies of all of the fibrils formed from the cross-seeding experiments with the mutational variants were observed to be very similar (~7 nm in diameter; *SI Appendix*, Fig. S5*A*).

The Rate of Fibril Amplification of α-Synuclein Under Mildly Acidic pH Conditions Is Strongly Influenced by the Mutations. We next performed sets of cross-seeding experiments (Fig. 4*A* and *SI Appendix*, Fig. S6) at mildly acidic pH and under quiescent conditions, where α-synuclein fibrils have been shown to amplify autocatalytically and to form higher order assemblies (20). Under these conditions, the observed change in the overall aggregation rate (see *SI Appendix*, Eq. **10**) is therefore attributable to the simultaneous changes in the monomer concentration and the number of growing fibrils, the latter being the sum of processes that increase and decrease the number of fibril ends [i.e., secondary nucleation and higher order assembly (20), respectively].

The results show that under these conditions the A30P, E46K, and A53T variants, like the WT protein (20, 37), show sigmoidal aggregation profiles, which are indicative of the contribution of secondary nucleation to the growth kinetics, and that are independent of the specific variant from which the seed fibrils are formed (Fig. 4 *A* and *B* and *SI Appendix*, Fig. S6). Detailed analysis of these data shows that the rates of fibril amplification (*SI Appendix*, Fig. S7*A*) for the WT, A30P, E46K, and A53T variants are within an order of magnitude of each other and that the reaction half times (*SI Appendix*, Fig. S7*B*) display only a weak dependence on the initial monomer concentration in the range studied in the present work; this finding suggests that in each of these cases, the autocatalytic process is independent of the monomer concentration, which could, for example, be the result of the saturation of all of the effective nucleation sites on the surfaces of the fibrils (43). The behavior of the H50Q and G51D variants is, however, very different from that of the WT protein as only very slow aggregation is observed for these variants (Fig. 4 and *SI Appendix*, Fig. S6). To be able to distinguish whether this striking difference in behavior originates from differences in the rates of elongation or secondary nucleation under these conditions, we carried out experiments at higher seed concentrations at acidic pH. Here, the depletion of monomeric protein molecules through fibril elongation is so rapid that secondary nucleation does not detectably contribute to the aggregation process, as suggested by the exponential, rather than sigmoidal kinetic curves. We found that the elongation rates, although significantly faster than at neutral pH (20), are the same within an order of magnitude for all variants (*SI Appendix*, Fig. S8). Taken together, these findings suggest that the α-synuclein variants H50Q and G51D have a very slow secondary nucleation rate. The amino acid substitutions in each of the two variants (H for Q and G for D) imply a change in the net charge from that of the WT protein under these conditions, and so we probed the pH dependence of their aggregation rates at pH values between 7.4 and 5.2, at both low and high seed concentrations. We did not detect aggregation at low seed concentrations for either H50Q or G51D under these conditions (*SI Appendix*, Fig. S9 *A* and *B*), suggesting the absence of notable secondary nucleation throughout this pH range. At higher seed concentrations, we found that the elongation rate increased in magnitude, notably from pH 6.6 to pH 5.8 (*SI Appendix*, Fig. S9 *C*–*E*), a behavior very similar to that reported for the WT protein (20). The very low aggregation rates for the H50Q and G51D variants at low seed concentrations and acidic pH, therefore, indicate a negligible rate of aggregate formation through secondary nucleation.

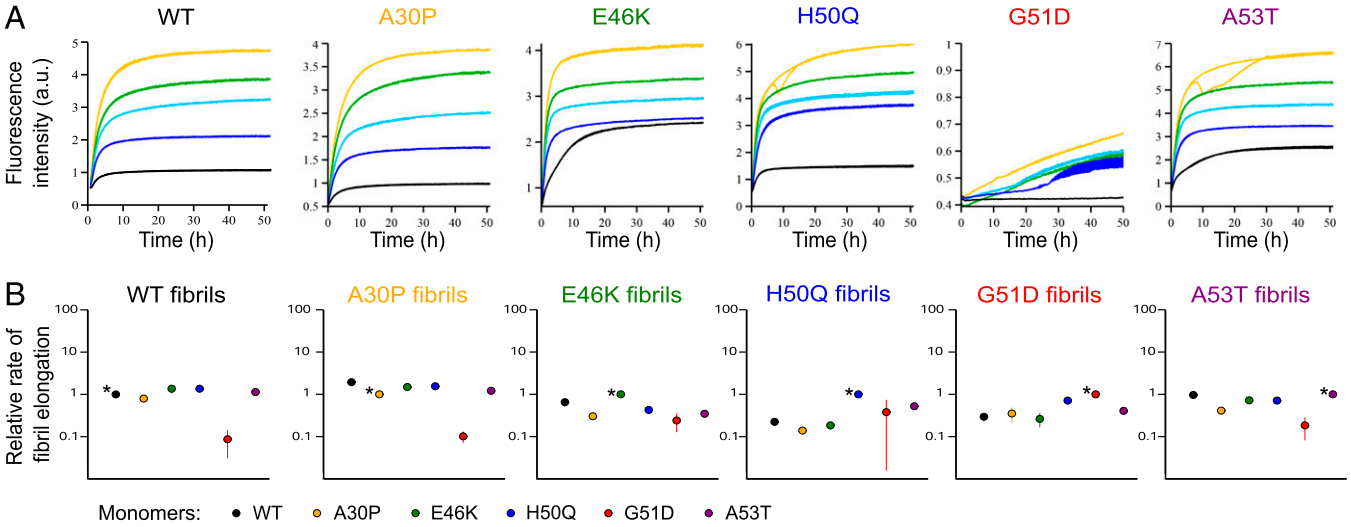

Fig. 3. The elongation rate of α-synuclein is only mildly affected by the disease-associated mutations. (*A*) Change in ThT fluorescence when monomeric α-synuclein at different concentrations [10 μM (black), 30 μM (blue), 50 μM (light blue), 70 μM (green), and 100 μM (yellow)] was incubated in the presence of 5 μM preformed fibrils of the WT protein under quiescent conditions at pH 6.5 and 37 °C. a.u., arbitrary units. (*B*) Normalized ratios of the elongation rates of the disease-associated variants relative to that of each variant monomer elongating its own preformed fibrils. Note that the elongation of seeds by monomers of the same type (marked by *) is always among the fastest (except for A30P).

Discussion

Although the biological function of α-synuclein has not yet been elucidated in detail, suggestions include, among others, the regulation of vesicular plasticity (40), oxidative stress, and mitochondrial function (41). Furthermore, α-synuclein has been shown to experience heterogeneous cellular environments, including differences in pH ranging from 5.5 to 7.4 (2–7, 40, 41). In the light of these findings, and of our knowledge of the high dependence of α-synuclein aggregation on the pH of its environment (20, 37) and on the presence of surfaces (21, 36), we have developed a comprehensive strategy to further our overall understanding of the way that α-synuclein converts from its normally soluble state into amyloid fibrils. This strategy involves studying separately the different processes involved in the aggregation reaction, namely the initial formation steps, the growth of the fibrils, and their amplification (Figs. 2–4). Our approach relies on the presence of a variety of features to induce aggregation, such as negatively charged lipids or acidic solution conditions, and represents a step toward a characterization of amyloid formation by α-synuclein that is relevant to key aspects of physiological conditions.

This approach has been applied in the present study to characterize the effects of five mutational variants, namely A30P, E46K, H50Q, G51D, and A53T, in α-synuclein that are associated with familial Parkinson's disease (14–18). Our results show that single-amino acid substitutions in the 140-residue chain of α-synuclein not only increase or decrease the overall rate of

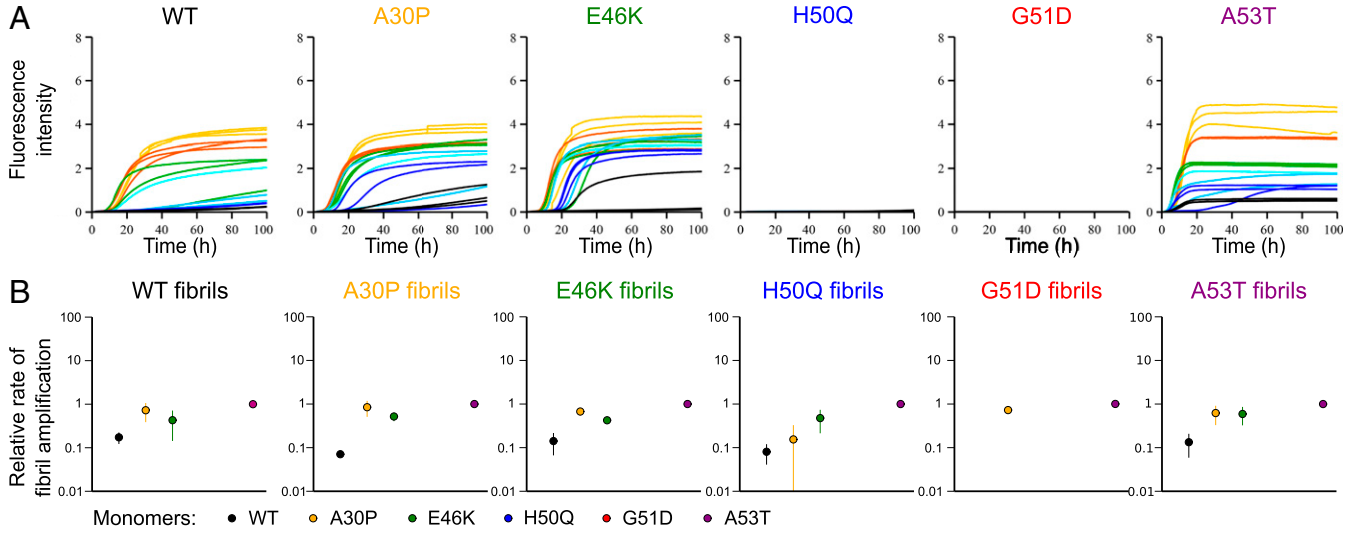

Fig. 4. The rates of fibril amplification of WT α-synuclein, A30P, E46K, and A53T, but not that of H50Q and G51D, are enhanced at mildly acidic pH. (*A*) Change in ThT fluorescence intensity when monomeric α-synuclein (WT, A30P, E46K, H50Q, G51D, and A53T) was incubated in the presence of 35 nM preformed fibrils of the WT protein under quiescent conditions at pH 4.8 and 37 °C. The protein concentrations used in this study were 20 μM (black), 30 μM (dark blue), 40 μM (light blue), 50 μM (green), 70 μM (red), and 100 μM (yellow). (*B*) The relative rates of fibril amplification of the α-synuclein variants were averaged over the concentrations studied here and normalized relative to the rate of the fastest aggregating monomeric variant (i.e., A53T α-synuclein).

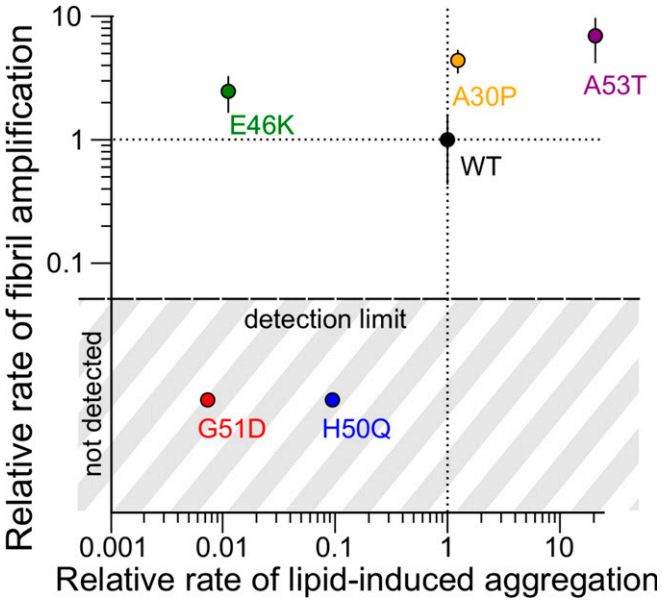

Fig. 5. Mutations associated with familial Parkinson's disease alter the lipid-induced aggregation and fibril amplification steps of α-synuclein amyloid formation. The plot summarizes the effects of the five single-amino acid mutations studied in this work on the rates of lipid-induced aggregation and fibril amplification at mildly acidic pH. The data were normalized relative to the rates of WT (black circle) α-synuclein.

aggregation, as noted in earlier studies (22–30) and as reproduced by us (*SI Appendix*, Fig. S10), but also dramatically affect the relative importance of individual microscopic steps (Fig. 5). More specifically, our findings indicate that the process of fibril elongation by addition of monomeric protein molecules to preformed fibrils is only relatively weakly affected by the mutations, with the measured rates spanning less than one order of magnitude (*SI Appendix*, Fig. S11). The data reveal, however, that the elongation rates of E46K, H50Q, G51D, and A53T are faster for monomeric proteins that add to fibrils formed by the same sequence compared with those formed from different variants (Fig. 3). All of those sequence changes are located well within the region of the α-synuclein sequence that is thought to make up the cross-β core of the amyloid fibrils [ca. residues 30–110 (44, 45)].

Although the fibril elongation step in the aggregation of α-synuclein is not very strongly influenced by the disease-associated single point mutations, we find that the rate of surface-induced fibril production processes, via interaction with lipid vesicles or fibril surfaces at mildly acidic pH, can be dramatically affected by these sequence modifications (Fig. 5). Indeed, the rate of lipid-induced aggregation was found to vary by three orders of magnitude across the five variants (Figs. 2*H* and 5) with values both higher (A53T) and lower (E46K, H50Q, and G51D) than that of the WT protein; these findings are consistent with previous descriptions of the overall relative rates of aggregation under nonquiescent reaction conditions where surface effects are also likely to be dominant (22, 31).

These observations reveal that lipid-induced generation of fibrils is highly sensitive to the specific sequence of the protein, in particular, the region encompassing the residues 46–51. Similar effects on the aggregation rate are also evident at mildly acidic pH, where secondary nucleation and higher-order assembly processes are strongly enhanced (20). In particular, the rates of fibril amplification for A53T, A30P, E46K, and WT α-synuclein were observed to be within an order of magnitude of each other, whereas the rates of secondary nucleation were found to be undetectably slow for H50Q and G51D (Fig. 4), suggesting that a decrease in charge from +1 to 0 or from 0 to −1 in this region interferes with the secondary nucleation process. Overall, we note that the rates of individual microscopic steps in the process can differ by several orders of magnitude between different variants, whereas in previous reports under shaking conditions, the observed differences appear to be much smaller. This effect is likely to stem from the fact that shaking leads not only to enhanced primary nucleation rates (37) but also to strongly enhanced rates of aggregate fragmentation that are likely to be rate determining in such cases (46). The latter effect, therefore, is likely to mask, at least in part, the intrinsic differences in the nucleation rate constants.

Because both lipid-induced fibril production and secondary nucleation of α-synuclein aggregation are heterogeneous processes [i.e., they occur on surfaces (of lipid vesicles and fibrils, respectively)], it is interesting to ask whether these two types of events are effectively the same process occurring on different surfaces or if they are fundamentally different events. We find that mutations associated with a change in the protonation state of the protein induce a change either in the rate of the lipid-induced aggregation alone [E46K (+2)] or in the rates of both surface-induced fibril production processes [H50Q (−1) and G51D (−1)] (Fig. 5), suggesting that the two types of processes are significantly different. However, given that these nucleation events are both linked to a pre-equilibrium of α-synuclein binding to the respective surfaces, such differences could be caused by differential surface binding affinity or else by differences in the nucleation event itself. In any case, our results suggest that electrostatic interactions play an important role in the various nucleation events.

Translating these findings into a medically relevant context is, however, far from straightforward, not least because of the large variations in the ages of onset reported for even the same familial forms of Parkinson's disease (19). Moreover, biological processes such as the pathways by which wild-type α-synuclein is normally degraded were shown to be affected by some of the disease-associated mutations (A30P and A53T), leading to the accumulation of the corresponding mutants and a gain of their toxicity (47). Finally, the lack of a simple correlation between the in vitro aggregation propensity and the age of disease onset reinforces the view that cellular factors are able to modulate the intrinsic aggregation propensities that are defined by the amino acid sequence.

In summary, the present work represents a detailed analysis of the influence of mutations associated with familial Parkinson's disease on the different microscopic steps in the process of α-synuclein aggregation. In particular, our results show that the ability of a given sequence to elongate preformed seed fibrils is affected only to a relatively small degree by the identities of the monomeric and fibrillar variants. By contrast, the rates of the processes responsible for the de novo production of fibrils (lipid-induced aggregation and secondary nucleation) have been found to differ by multiple orders of magnitude depending on which mutational variant is involved in monomeric form. In conclusion, the results reveal that single-point mutations in α-synuclein can lead to dramatic changes in the balance of the individual molecular steps of α-synuclein aggregation and hence in the overall mechanism of amyloid formation.

Materials and Methods

Detailed information on experimental measurements and on methods of kinetic analysis can be found in *SI Appendix*. WT α-synuclein and the mutational variants were expressed and purified as previously described (20). Lipid vesicles were prepared by freeze–thaw cycles and sonication (21). Differential scanning calorimetry thermograms were acquired using a Microcal VP-DSC calorimeter. Far-UV circular dichroism spectra were recorded on a JASCO J-810 spectrophotometer. Aggregation experiments were performed in low-binding, clear-bottomed half-area 96-well plates under quiescent conditions and amyloid formation was monitored by the increase in ThT fluorescence. Atomic force microscopy images were obtained with a Nanowizard II atomic force microscope using tapping mode in air.

ACKNOWLEDGMENTS. We acknowledge support from the Boehringer Ingelheim Fonds (P.F.); the Cambridge Home and European Union Scholarship Scheme (G.M.); the Leverhulme Trust and the Magdalene College, Cambridge (A.K.B.); the Frances and Augustus Newman Foundation (T.P.J.K.); the UK Biotechnology and Biochemical Sciences Research Council (C.M.D. and M.V.); the Wellcome Trust (C.M.D., T.P.J.K., and M.V.); and the Cambridge Centre for Misfolding Diseases (P.F., G.M., M.V., T.P.J.K., C.M.D., A.K.B., and C.G.).

1. Kim WS, Kågedal K, Halliday GM (2014) α-Synuclein biology in Lewy body diseases. *Alzheimers Res Ther* 6(5):73.
2. Nakajo S, et al. (1990) Purification and characterization of a novel brain-specific 14-kDa protein. *J Neurochem* 55(6):2031–2038.
3. Shibayama-Imazu T, et al. (1993) Cell and tissue distribution and developmental change of neuron specific 14 kDa protein (phosphoneuroprotein 14). *Brain Res* 622(1-2):17–25.
4. Stefanis L (2012) α-Synuclein in Parkinson's disease. *Cold Spring Harb Perspect Med* 2(2):a009399.
5. Iwai A, et al. (1995) The precursor protein of non-A β component of Alzheimer's disease amyloid is a presynaptic protein of the central nervous system. *Neuron* 14(2): 467–475.
6. Maroteaux L, Campanelli JT, Scheller RH (1988) Synuclein: A neuron-specific protein localized to the nucleus and presynaptic nerve terminal. *J Neurosci* 8(8):2804–2815.
7. Lotharius J, Brundin P (2002) Impaired dopamine storage resulting from α-synuclein mutations may contribute to the pathogenesis of Parkinson's disease. *Hum Mol Genet* 11(20):2395–2407.
8. Gundelfinger ED, Kessels MM, Qualmann B (2003) Temporal and spatial coordination of exocytosis and endocytosis. *Nat Rev Mol Cell Biol* 4(2):127–139.
9. Atluri PP, Ryan TA (2006) The kinetics of synaptic vesicle reacidification at hippocampal nerve terminals. *J Neurosci* 26(8):2313–2320.
10. Sinning A, Hübner CA (2013) Minireview: pH and synaptic transmission. *FEBS Lett* 587(13):1923–1928.
11. Forgac M (2007) Vacuolar ATPases: Rotary proton pumps in physiology and pathophysiology. *Nat Rev Mol Cell Biol* 8(11):917–929.
12. Masliah E, et al. (2005) Effects of alpha-synuclein immunization in a mouse model of Parkinson's disease. *Neuron* 46(6):857–868.
13. Spillantini MG, Crowther RA, Jakes R, Hasegawa M, Goedert M (1998) α-Synuclein in filamentous inclusions of Lewy bodies from Parkinson's disease and dementia with lewy bodies. *Proc Natl Acad Sci USA* 95(11):6469–6473.
14. Polymeropoulos MH, et al. (1997) Mutation in the α-synuclein gene identified in families with Parkinson's disease. *Science* 276(5321):2045–2047.
15. Krüger R, et al. (1998) Ala30Pro mutation in the gene encoding α-synuclein in Parkinson's disease. *Nat Genet* 18(2):106–108.
16. Zarranz JJ, et al. (2004) The new mutation, E46K, of α-synuclein causes Parkinson and Lewy body dementia. *Ann Neurol* 55(2):164–173.
17. Proukakis C, Houlden H, Schapira AH (2013) Somatic α-synuclein mutations in Parkinson's disease: Hypothesis and preliminary data. *Mov Disord* 28(6):705–712.
18. Lesage S, et al.; French Parkinson's Disease Genetics Study Group (2013) G51D α-synuclein mutation causes a novel parkinsonian-pyramidal syndrome. *Ann Neurol* 73(4):459–471.
19. Fujioka S, et al. (2014) Update on novel familial forms of Parkinson's disease and multiple system atrophy. *Parkinsonism Relat Disord* 20(Suppl 1):S29–S34.
20. Buell AK, et al. (2014) Solution conditions determine the relative importance of nucleation and growth processes in α-synuclein aggregation. *Proc Natl Acad Sci USA* 111(21):7671–7676.
21. Galvagnion C, et al. (2015) Lipid vesicles trigger α-synuclein aggregation by stimulating primary nucleation. *Nat Chem Biol* 11(3):229–234.
22. Conway KA, et al. (2000) Acceleration of oligomerization, not fibrillization, is a shared property of both α-synuclein mutations linked to early-onset Parkinson's disease: Implications for pathogenesis and therapy. *Proc Natl Acad Sci USA* 97(2):571–576.
23. Narhi L, et al. (1999) Both familial Parkinson's disease mutations accelerate α-synuclein aggregation. *J Biol Chem* 274(14):9843–9846.
24. Li J, Uversky VN, Fink AL (2001) Effect of familial Parkinson's disease point mutations A30P and A53T on the structural properties, aggregation, and fibrillation of human α-synuclein. *Biochemistry* 40(38):11604–11613.
25. Lashuel HA, et al. (2002) α-synuclein, especially the Parkinson's disease-associated mutants, forms pore-like annular and tubular protofibrils. *J Mol Biol* 322(5):1089–1102.
26. Li J, Uversky VN, Fink AL (2002) Conformational behavior of human α-synuclein is modulated by familial Parkinson's disease point mutations A30P and A53T. *Neurotoxicology* 23(4-5):553–567.
27. Fredenburg RA, et al. (2007) The impact of the E46K mutation on the properties of α-synuclein in its monomeric and oligomeric states. *Biochemistry* 46(24):7107–7118.
28. Lemkau LR, et al. (2012) Mutant protein A30P α-synuclein adopts wild-type fibril structure, despite slower fibrillation kinetics. *J Biol Chem* 287(14):11526–11532.
29. Ghosh D, et al. (2013) The Parkinson's disease-associated H50Q mutation accelerates α-Synuclein aggregation in vitro. *Biochemistry* 52(40):6925–6927.
30. Khalaf O, et al. (2014) The H50Q mutation enhances α-synuclein aggregation, secretion, and toxicity. *J Biol Chem* 289(32):21856–21876.
31. Fares MB, et al. (2014) The novel Parkinson's disease linked mutation G51D attenuates in vitro aggregation and membrane binding of α-synuclein, and enhances its secretion and nuclear localization in cells. *Hum Mol Genet* 23(17):4491–4509.
32. Dobson CM (2003) Protein folding and misfolding. *Nature* 426(6968):884–890.
33. Knowles TP, Vendruscolo M, Dobson CM (2014) The amyloid state and its association with protein misfolding diseases. *Nat Rev Mol Cell Biol* 15(6):384–396.
34. Cohen SI, Vendruscolo M, Dobson CM, Knowles TP (2012) From macroscopic measurements to microscopic mechanisms of protein aggregation. *J Mol Biol* 421(2-3): 160–171.
35. Grey M, et al. (2015) Acceleration of α-synuclein aggregation by exosomes. *J Biol Chem* 290(5):2969–2982.
36. Vácha R, Linse S, Lund M (2014) Surface effects on aggregation kinetics of amyloidogenic peptides. *J Am Chem Soc* 136(33):11776–11782.
37. Grey M, Linse S, Nilsson H, Brundin P, Sparr E (2011) Membrane interaction of α-synuclein in different aggregation states. *J Parkinsons Dis* 1(4):359–371.
38. Galvagnion C, et al. (2016) Chemical properties of lipids strongly affect the kinetics of the membrane-induced aggregation of α-synuclein. *Proc Natl Acad Sci USA* 113(26): 7065–7070.
39. Wood SJ, et al. (1999) α-synuclein fibrillogenesis is nucleation-dependent. Implications for the pathogenesis of Parkinson's disease. *J Biol Chem* 274(28):19509–19512.
40. Clayton DF, George JM (1998) The synucleins: A family of proteins involved in synaptic function, plasticity, neurodegeneration and disease. *Trends Neurosci* 21(6):249–254.
41. Bonini NM, Giasson BI (2005) Snaring the function of α-synuclein. *Cell* 123(3):359–361.
42. Fusco G, et al. (2014) Direct observation of the three regions in α-synuclein that determine its membrane-bound behaviour. *Nat Commun* 5:3827.
43. Meisl G, et al. (2014) Differences in nucleation behavior underlie the contrasting aggregation kinetics of the Aβ40 and Aβ42 peptides. *Proc Natl Acad Sci USA* 111(26): 9384–9389.
44. Miake H, Mizusawa H, Iwatsubo T, Hasegawa M (2002) Biochemical characterization of the core structure of α-synuclein filaments. *J Biol Chem* 277(21):19213–19219.
45. Vilar M, et al. (2008) The fold of α-synuclein fibrils. *Proc Natl Acad Sci USA* 105(25): 8637–8642.
46. Knowles TP, et al. (2009) An analytical solution to the kinetics of breakable filament assembly. *Science* 326(5959):1533–1537.
47. Cuervo AM, Stefanis L, Fredenburg R, Lansbury PT, Sulzer D (2004) Impaired degradation of mutant alpha-synuclein by chaperone-mediated autophagy. *Science* 305(5688):1292–1295.

SI Appendix: Mutations associated with familial Parkinson's disease alter the initiation and amplification steps of α-synuclein aggregation

Patrick Flagmeier[a], Georg Meisl[a], Michele Vendruscolo[a], Tuomas P.J. Knowles[a], Christopher M. Dobson[a,1], Alexander K. Buell[a,b,1], and Céline Galvagnion[a,1]

[a]Department of Chemistry, University of Cambridge, Lensfield Road, Cambridge CB2 1EW, UK; [b]Present address: Institute of Physical Biology, University of Düsseldorf, Universitätsstr.1, 40225 Düsseldorf, Germany; [1]To whom correspondence should be addressed. E-mail: cmd44@cam.ac.uk, Alexander.Buell@uni-duesseldorf.de, cg393@cam.ac.uk

1. SI Methods

Reagents. Thioflavin T UltraPure Grade (ThT > 95%) was purchased from Eurogentec Ltd (Belgium). Sodium phosphate monobasic (NaH_2PO_4, BioPerformance Certified > 99.0%), sodium phosphate dibasic (Na_2 HPO_4, ReagentPlus, > 99.0%) and sodium azide (NaN_3, ReagentPlus, > 99.5%) were purchased from Sigma Aldrich, UK. 1,2-Dimyristoyl-sn-glycero-3-phospho-L-serine, sodium salt (DMPS) was purchased from Avanti Polar Lipids, Inc, USA.

Protein preparation. α-synuclein variants were expressed and purified as described previously [1–3]. To determine the concentrations in solution we used the absorbance value of the protein measured at 275 nm and an extinction coefficient of 5,600 M^{-1}. The protein solutions were divided into aliquots, flash frozen in liquid N_2 and stored at -80°C, until required for use.

Seed fibril formation. Seed fibrils were produced as described previously [1]. 500 μL samples of α-synuclein at concentrations from 500-800 μM were incubated in 20 mM phosphate buffer (pH 6.5) for 48-72 h at ca. 40°C and stirred at 1,500 rpm with a Teflon bar on an RCT Basic Heat Plate (IKA, Staufen, Germany). Fibrils were diluted to a monomer equivalent concentration of 200 μM, divided into aliquots, flash frozen in liquid N_2 and stored at -80°C. For experiments at pH 6.5 and μM fibril concentrations the 200 μM fibril stock was sonicated for between 0.5 and 1 min using a probe sonicator (Bandelin, Sonopuls HD 2070, Berlin, Germany), using 10% maximum power and a 50% cycle. For experiments at low pH with nM fibril concentrations the 200 μM stock was diluted to 10 μM in water, sonicated 3 times for 5 s using 10% maximum power and 50% cycles using the probe sonicator.

Lipid vesicle preparation. DMPS lipid powder was dissolved in 20 mM phosphate buffer (NaH_2PO_4 /Na_2HPO_4), pH 6.5, 0.01% NaN_3 and stirred at 45°C for at least 2 h. The solutions were then frozen and thawed five times using dry ice and a water bath at 45°C. Lipid vesicles were prepared by sonication (Bandelin, Sonopuls HD 2070, 3 x 5 min, 50% cycle, 10% maximum power) and centrifuged at 15,000 rpm for 30 min at 25°C. The average size of the vesicles was checked by

dynamic light scattering (Zetasizer Nano ZSP, Malvern Instruments, Malvern, UK) to ensure a distribution centered at a diameter of 20 nm.

AFM images and analysis. Atomic force microscopy images were taken using a Nanowizard II atomic force microscope (JPK, Berlin, Germany) using tapping mode in air. Solutions containing fibrils were diluted to a monomer concentration of 1 μM in water and 10 μL samples of the diluted solution were deposited on freshly cleaved mica and left to dry for at least 30 min. The samples were carefully washed with 50 μL of water and then dried again. The images were loaded into the freely available software Gwyddion and the profile function was used to extract a height profile. To determine the fibril thickness the baseline height of the image was subtracted from the fibril height.

CD spectroscopy. CD samples were prepared by incubating 20 μM WT α-synuclein or each of the different variants in the presence of increasing concentrations of DMPS in 20 mM phosphate buffer, pH 6.5. Far-UV CD spectra were recorded on a JASCO J-810 spectrophotometer (JASCO UK, Ltd) equipped with a Peltier thermally controlled cuvette holder at 30°C. Quartz cuvettes with path lengths of 1 mm were used and CD spectra were obtained by averaging five individual spectra recorded between wavelengths of 250 and 200 nm, with a bandwidth of 1 nm, a data pitch of 0.2 nm, a scanning speed of 50 nm/min, and a response time of 1 s. Each value of the CD signal intensity reported at 222 nm corresponds to the average of 60 measurements. For each protein sample, the CD signal of the buffer used to solubilize the protein was recorded and subtracted from the CD signal of the protein. The CD data were analyzed as previously described [2]. In brief, the observed CD signal (CD_{obs}) consists of the sum of the signals of the lipid-bound and free α-synuclein:

$$CD_{obs} = x_{\alpha-syn_B} CD_B + x_{\alpha-syn_F} CD_F \quad [1]$$

where $x_{\alpha-syn_B}$ and $x_{\alpha-syn_F}$ are the fractions of α-synuclein bound to the membrane and free in solution, respectively, and CD_B and CD_F are the CD signals of the bound and free forms of α-synuclein, respectively. By assuming that $x_{\alpha-syn_B} + x_{\alpha-syn_F} = 1$, and that the signals of α-synuclein in the presence of buffer, or in the presence of model membranes under saturating conditions, correspond to CD_F and CD_B, respectively, the fraction of α-synuclein bound to SUV for each sample can be expressed as:

$$x_{\alpha-syn_B} = \frac{CD_{obs} - CD_F}{CD_B - CD_F} \quad [2]$$

We used the following model: $\alpha - \mathrm{syn} + \mathrm{lipid}_\mathrm{L} \rightleftharpoons \alpha - \mathrm{syn}(\mathrm{lipid})_\mathrm{L}$, which corresponds to a non-cooperative binding Langmuir-Hill adsorption model, and the following equation to fit the measured CD signal:

$$x_{\alpha-syn_B} = \frac{([\alpha - syn] + \frac{[lipid]}{L} + K_D) - \sqrt{([\alpha - syn] + \frac{[lipid]}{L} + K_D)^2 - \frac{4[lipid][\alpha-syn]}{L}}}{2[\alpha - syn]} \quad [3]$$

where K_D (in M) is the dissociation constant and L is the number of lipid molecules interacting with one molecule of α-synuclein.

Differential scanning calorimetry. DSC thermograms were acquired using a Microcal VP-DSC calorimeter (Malvern Instruments, Malvern, UK) with a scanning rate of $1°C.min^{-1}$. Protein and lipid samples were degassed for 20 min at room temperature prior to the measurements. For each sample, the DSC thermogram of the buffer was subtracted from that of the sample.

Measurement of aggregation kinetics. WT α-synuclein or its variants were incubated at the concentrations indicated and in the presence of 50 μM ThT and either preformed fibrils or DMPS vesicles at 37°C or 30°C, respectively [1, 2]. The change in the ThT fluorescence signal was monitored using a Fluostar Optima or Polarstar Omega fluorescence plate reader (BMG Labtech, Aylesbury, UK) in bottom reading mode under quiescent conditions. Corning 96 well plates with half-area (3881, polystyrene, black with clear bottom) non-binding surfaces sealed with metal sealing tape were used for each experiment. For experiments involving shaking (orbital shaking for 300 s at 1,100 rpm), glass beads were introduced in the wells of the plate prior to the measurement and the change in the ThT fluorescence signal was monitored using a Polarstar Omega fluorescence plate reader. At the end of each aggregation experiment the concentrations of monomeric and fibrillar states of the protein were determined as described previously [2].

2. SI Analysis of the aggregation kinetics

Determination of the lipid-induced aggregation rate.

Kinetic analysis of the early time points of the aggregation curves of WT α-synuclein and of the A30P, E46K, H50Q, A53T variants. The change in mass concentration of fibrils with time M(t) was fitted [4] using the model described previously [2] and the following equation:

$$M(t) = \frac{K_M k_+ m(0)^{n+1} k_n b t^2}{2(K_M + m(0))} \quad [4]$$

where k_+ is the elongation rate constant of fibrils from lipid vesicles, k_n is the heterogeneous primary nucleation rate constant, n is the reaction order of the heterogeneous primary nucleation reaction relative to the free monomer, m, b is the total mass concentration of the protein bound to the lipid at 100% coverage ($b = \frac{[\mathrm{DMPS}]}{L}$, with L the stoichiometry) and K_M is the Michaelis constant (fixed at 125 μM for each mutant, as determined previously [2]). This global analysis yields $k_n k_+$ and n, for each variant. We then estimated the rate of aggregation of each variant on lipid vesicles, $\left(\frac{dM(t)}{dt}\right)_{\mathrm{variant}} = \frac{K_M k_+ k_{n,\mathrm{variant}} b m_{\mathrm{variant}}(0)^{n,\mathrm{variant}} t}{4(K_M + m_{\mathrm{variant}}(0))}$, relative to that of the WT protein, for the same initial concentrations of free monomer and monomer bound to the lipid, i.e. $m_{\mathrm{variant}}(0) = m_{\mathrm{WT}}(0)$ and $b_{\mathrm{variant}} = b_{\mathrm{WT}}$, respectively, using the following equation:

$$\text{Relative rate of aggregation on vesicles} = \frac{\left(\frac{dM(t)}{dt}\right)_{\mathrm{variant}}}{\left(\frac{dM(t)}{dt}\right)_{\mathrm{WT}}} = \frac{(k_n k_+)_{\mathrm{variant}} m(0)^{n,\mathrm{variant}}}{(k_n k_+)_{\mathrm{WT}} m(0)^{n,\mathrm{WT}}} \quad [5]$$

Determination of the upper bound of the relative rate of lipid-induced aggregation of G51D α-synuclein. Our data suggest that the G51D variant does not form detectable fibrils even when the protein is incubated for 65 h in the presence of 100 μM DMPS. We have shown previously that the upper bound of the concentration of fibrils that can be detected using our ThT assay is 0.4 μM [2]. We therefore estimated the upper limit of $\left(\frac{dM(t)}{dt}\right)_{\mathrm{G51D}} = \frac{K_M k_+ k_{n,\mathrm{G51D}} b m(0)^{n,\mathrm{G51D}} t}{4(K_M + m(0))}$ using equation 4 and the following values for the various constants: $M(t) \leq 0.4$ μM, $m(0) = 100$ μM, $b = 3.3$ μM, $t = 65$ h. We then used this value to determine the upper bound of the relative rate of aggregation on vesicles to that of the WT protein by using equation 5.

Derivation of the approach used to analyze highly seeded aggregation data. For aggregation experiments at high seed concentrations (μM), under which primary nucleation of α-synuclein can be neglected, and under quiescent conditions, where fragmentation is negligible, the aggregation kinetics for the consumption of monomers can be described by the equation:

$$\frac{dm(t)}{dt} = -\frac{dM(t)}{dt} = -2k_+ P(t) m(t) \quad [6]$$

where k_+ is the fibril elongation rate constant, $m(t)$ the monomer concentration, M(t) is the mass concentration of fibrils and $P(t)$ the number concentration of fibrils. At early times in the aggregation reaction, the monomer concentration and the fibril number concentration can be assumed to be constant, hence $m(t) = m(0)$ and $P(t) = P(0)$, and:

$$\left.\frac{dM(t)}{dt}\right|_{t=0} = 2k_+ P(0) m(0) \quad [7]$$

By fitting a linear slope to the early time points of the aggregation reaction, we can obtain the value of $2k_+P(0)m(0)$. For the comparison of the rate constants of different variants, we then calculate ratios r:

$$r = \frac{\left(\frac{dM(t)}{dt}\right)_{j,i}\Big|_{t=0}}{\left(\frac{dM(t)}{dt}\right)_{i,i}\Big|_{t=0}} = \frac{2k_{+;j,i}P_i(0)m_j(0)}{2k_{+;i,i}P_i(0)m_i(0)} \quad [8]$$

r is the ratio of the initial gradient fitted to the kinetic trace for monomer j elongating from fibrils of variant i ($k_{+;j,i}$) and the initial gradient fitted to the kinetic trace for monomer i elongating from fibrils of variant i ($k_{+;i,i}$) (i.e. homogeneous elongation). $P_i(0)$ is the initial number concentration of fibrils from variant i and the same seed stock was used for all monomer variants. $m_j(0)$ and $m_i(0)$ are the initial monomer concentrations of variant j and variant i, respectively. Comparing elongation rates for monomeric proteins for the same initial monomeric protein concentration, i.e. $m_j(0) = m_i(0)$, elongating from fibrils of the same variant can be analyzed as:

$$r = \frac{\left(\frac{dM(t)}{dt}\right)_{j,i}\Big|_{t=0}}{\left(\frac{dM(t)}{dt}\right)_{i,i}\Big|_{t=0}} = \frac{k_{+;j,i}}{k_{+;i,i}} \quad [9]$$

Derivation of the approach to analyze aggregation kinetics at acidic pH. For aggregation experiments at low seed concentrations in 20 mM phosphate buffer under quiescent conditions at pH 4.8, the kinetic data can be analyzed in detail to determine the rate of amplification of α-synuclein fibrils. Under these conditions both primary nucleation and fragmentation are negligible, therefore, the rate of amplification of α-synuclein fibrils can be approximated to the change in the number concentration of fibrils, $\frac{dP(t)}{dt}$. The rate of autocatalytic amplification of α-synuclein fibrils was determined at the half-time of the reaction, so that we compare these rates for the same monomer concentration $m(t) = \frac{m(0)}{2}$. As for the previously described analysis of elongation rate constants, we start from the linear polymerization model:

$$\frac{dm(t)}{dt} = -\frac{dM(t)}{dt} = -2k_+P(t)m(t) \quad [10]$$

To analyze $\frac{dP(t)}{dt}$, we have to determine the derivative of $\frac{dM(t)}{dt}$,

$$\frac{d^2M(t)}{dt^2} = 2k_+\left(\frac{dm(t)}{dt}P(t) + \frac{dP(t)}{dt}m(t)\right) \quad [11]$$

which can then be rearranged to allow the calculation of $\frac{dP(t)}{dt}$:

$$\frac{dP(t)}{dt} = \frac{1}{2k_+m(t)}\left(\frac{d^2M(t)}{dt^2} - 2k_+\frac{dm(t)}{dt}P(t)\right) \quad [12]$$

At the half-time $\frac{d^2M(t)}{dt^2}$ is small for sigmoidal curves, therefore we assume that $\frac{d^2M(t)}{dt^2} \approx 0$, resulting in:

$$\frac{dP(t)}{dt}\Big|_{t=t_{1/2}} = -\frac{1}{m(t=t_{1/2})}P(t=t_{1/2})\,\frac{dm(t)}{dt}\Big|_{t=t_{1/2}} \quad [13]$$

It is defined that $m(t = t_{1/2}) = \frac{m(0)}{2}$. $P(t = t_{1/2})$ can be substituted by $-\frac{2}{m(0)k_+} \left.\frac{dm(t)}{dt}\right|_{t=t_{1/2}}$ using Eq. 10 resulting in:

$$\left.\frac{dP(t)}{dt}\right|_{t=t_{1/2}} = \left(\frac{1}{m(0)} \left.\frac{dm(t)}{dt}\right|_{t=t_{1/2}}\right)^2 \frac{4}{k_+} \quad [14]$$

$\left.\frac{dm(t)}{dt}\right|_{t=t_{1/2}}$ was determined from experimental data for WT, A30P, E46K and A53T α-synuclein by taking the first derivative of the sigmoidal fits to the kinetic traces shown in Fig. 4 and used to determine $\frac{dP(t)}{dt}$ for different monomer concentrations. $\frac{dP(t)}{dt}$ was then normalized to the rate of the fastest aggregating monomer variant A53T:

$$r = \frac{\left.\left(\frac{dP(t)}{dt}\right)_{j,i}\right|_{t=t_{1/2}}}{\left.\left(\frac{dP(t)}{dt}\right)_{\mathrm{A53T},i}\right|_{t=t_{1/2}}} = \frac{\left(\frac{1}{m_{j,i}(0)} \left.\left(\frac{dm(t)}{dt}\right)_{j,i}\right|_{t=t_{1/2}}\right)^2 \frac{1}{k_{+;j,i}}}{\left(\frac{1}{m_{\mathrm{A53T},i}(0)} \left.\left(\frac{dm(t)}{dt}\right)_{\mathrm{A53T},i}\right|_{t=t_{1/2}}\right)^2 \frac{1}{k_{+;\mathrm{A53T},i}}} \quad [15]$$

where $\left(\frac{dP(t)}{dt}\right)_{j,i}$ is the change in fibril number concentration for monomer variant j aggregating in the presence of pre-formed fibrils of variant i. $m_{j,i}(0)$ is the initial monomer concentration of monomer variant j aggregating in the presence of pre-formed fibrils of variant i. We found that the elongation rate in the presence of pre-formed fibrils is only marginally affected by the mutations (see above), therefore $k_{+;j,i} \approx k_{+;\mathrm{A53T},i}$ and since we form ratios for the same initial monomer concentration, we obtain $m_{j,i}(0) = m_{\mathrm{A53T},i}(0)$, further simplifying the analysis. Then the average of the ratios for each variant over the monomer concentrations can be defined as:

$$r = \frac{\left.\left(\frac{dP(t)}{dt}\right)_{j,i}\right|_{t=t_{1/2}}}{\left.\left(\frac{dP(t)}{dt}\right)_{\mathrm{A53T},i}\right|_{t=t_{1/2}}} = \left(\frac{\left.\left(\frac{dm(t)}{dt}\right)_{j,i}\right|_{t=t_{1/2}}}{\left.\left(\frac{dm(t)}{dt}\right)_{\mathrm{A53T},i}\right|_{t=t_{1/2}}}\right)^2 \quad [16]$$

1. Buell AK et al. (2014) Solution conditions determine the relative importance of nucleation and growth processes in α-synuclein aggregation. *Proc. Natl. Acad. Sci. U.S.A.* 111(21):7671–7676.
2. Galvagnion C et al. (2015) Lipid vesicles trigger α-synuclein aggregation by stimulating primary nucleation. *Nat. Chem. Biol.* 11(3):229–234.
3. Hoyer W et al. (2002) Dependence of alpha-synuclein aggregate morphology on solution conditions. *J. Mol. Biol.* 322(2):383–393.
4. Meisl G et al. (2016) Molecular mechanisms of protein aggregation from global fitting of kinetic models. *Nat Protoc* 11(2):252–272.

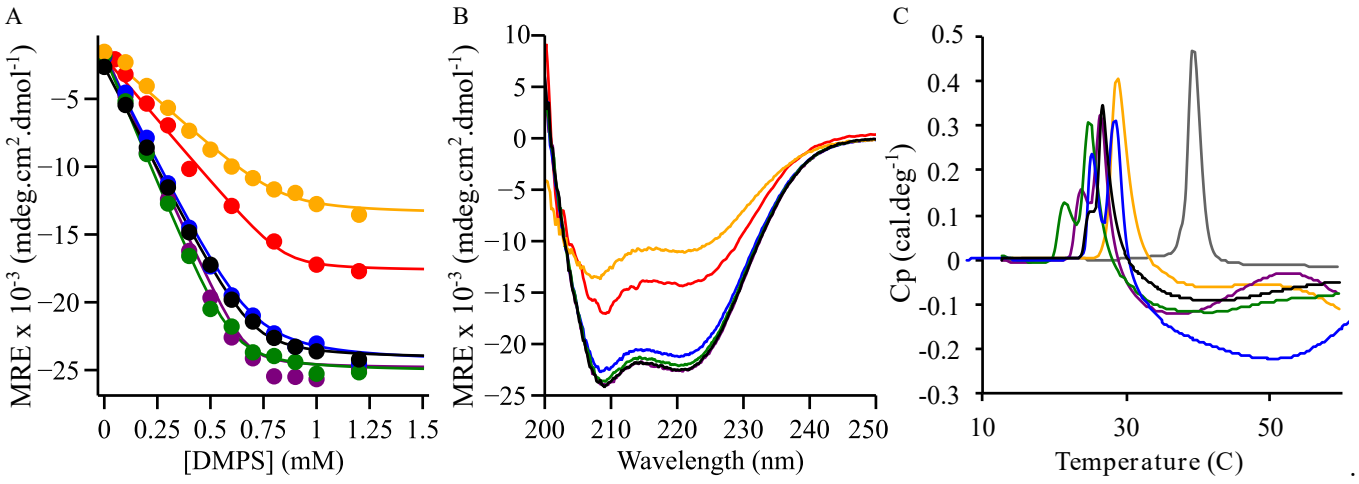

Fig. S1. Binding of WT and disease-associated variants of α-synuclein to DMPS vesicles. Change in the Mean Residue Ellipticity measured at 222 nm (A) and CD spectra (B) of α-synuclein (WT (black), A30P (yellow), E46K (green), H50Q (blue), G51D (red), A53T (purple)) measured at pH 6.5 and 30°C. The binding curves were fitted to a 1-step binding model (see Methods for details) and led to dissociation constants (K_D) of 0.38 $\pm$ 0.13 (WT), 0.55 $\pm$ 0.37 (A30P), 0.34 $\pm$ 0.20 (E46K), 0.61 $\pm$ 0.27 (H50Q), 0.16 $\pm$ 0.35 (G51D)and 0.18 $\pm$ 0.14 (A53T) μM and stoichiometries (L) of 28.2 $\pm$ 0.8 (WT), 33.2 $\pm$ 3.4 (A30P), 30.4 $\pm$ 1.6 (E46K), 35.2 $\pm$ 2.1 (H50Q), 42.5 $\pm$ 4.5 (G51D) and 26.7 $\pm$ 1.1 (A53T).(**C**) DSC traces of DMPS vesicles in the absence (grey) or the presence of WT (black), A30P (yellow), A53T (purple), E46K (green) or H50Q (blue) α-synuclein at pH 6.5.

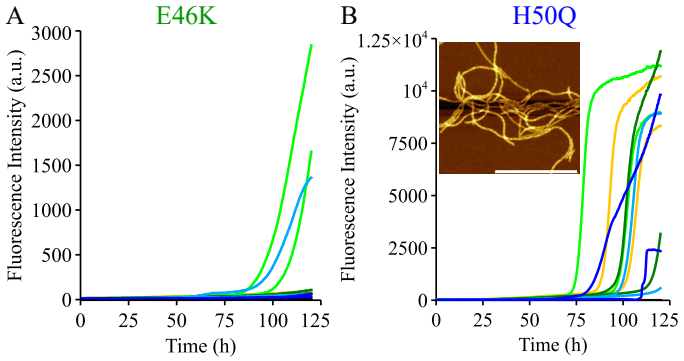

Fig. S2. DMPS induced aggregation of E46K and H50Q. (A,B) Change in ThT fluorescence intensity when α-synuclein (E46K (A), H50Q (B)) was incubated in the absence (black) and in the presence of 100 μM DMPS under quiescent conditions at pH 6.5 and 30°C. The protein concentrations used in this study were: 20 (dark blue), 40 (light blue), 60 (green), 80 (light green) and 100 μM (yellow). The inset of the panel B shows the AFM image of the fibrils formed under these conditions. The scale bar represents 1 μm.

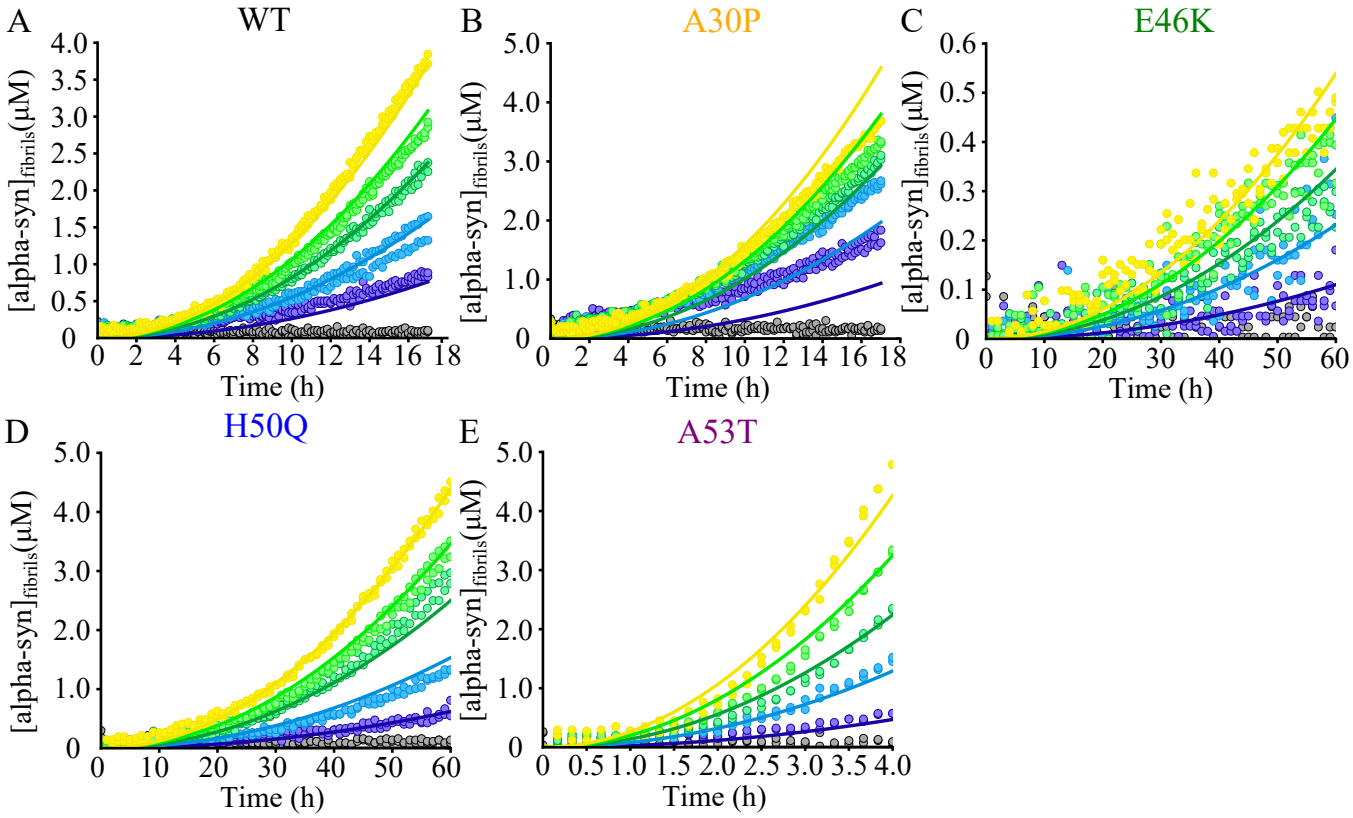

Fig. S3. Global analysis of WT and disease-associated variants of α-synuclein using a one-step nucleation model. Change in ThT fluorescence intensity when α-synuclein (WT (A), A30P (B), E46K (C), H50Q (D), A53T (E)) was incubated in the absence (black) and in the presence of 100 μM DMPS under quiescent conditions at pH 6.5 and 30°C. The protein concentrations used in this study were: 20 (dark blue), 40 (light blue), 60 (green), 80 (light green) and 100 μM (yellow). Global fitting of the early times of the aggregation curves to a one-step nucleation model leads to the determination of the product $k_n k_+$ ($1.2 \pm 0.6 \cdot 10^{-4}$ (WT), $1.47 \pm 0.03 \cdot 10^{-4}$ (A30P), $8.8 \pm 4 \cdot 10^{-7}$ (E46K), $9.3 \pm 1.8 \cdot 10^{-5}$ (H50Q), $8.3 \pm 0.3 \cdot 10^{-3}$ (A53T) $M^{-(n+1)}s^{-2}$, and n (0.26 ± 0.12 (WT), 0.26 (A30P), 0.22 ± 0.10 (E46K), 0.49 ± 0.04 (H50Q), 0.64 ± 0.01 (A53T)). K_M was fixed at 125 μM. The mean squared errors were: $1.1 \cdot 10^{-14}$ (WT), $1.9 \cdot 10^{-13}$ (A30P), $1.7 \cdot 10^{-15}$ (E46K), $1.3 \cdot 10^{-14}$ (H50Q), $1.3 \cdot 10^{-14}$ (A53T) μM^2.

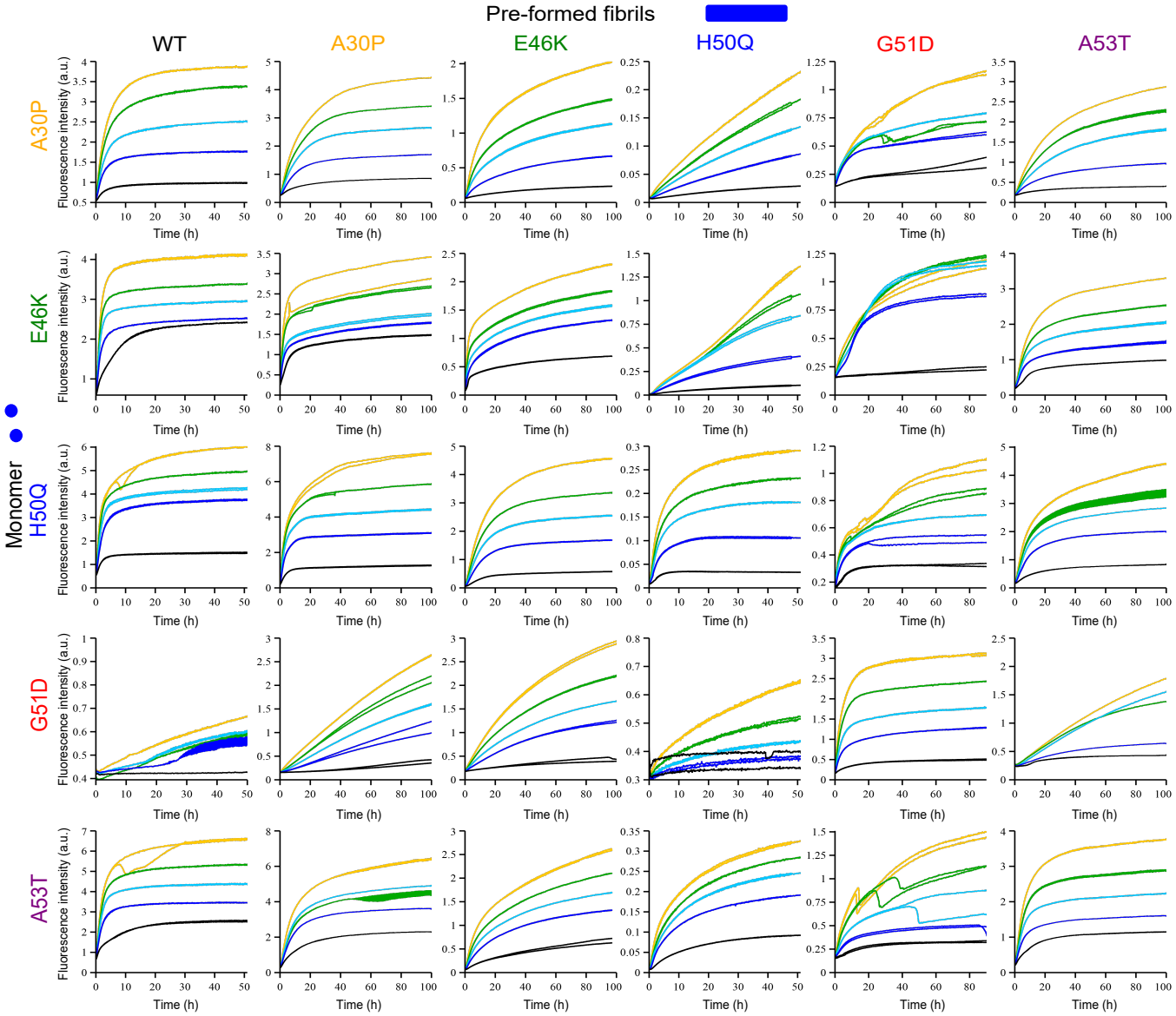

Fig. S4. Fibril elongation of WT α-synuclein and its disease-associated variants. Change in ThT fluorescence when monomeric α-synuclein at different concentrations (10 (black), 30 (blue), 50 (light blue), 70 (green) and 100 (yellow) μM) was incubated in the presence of 5 μM pre-formed fibrils from the indicated mutational variant (A30P, E46K, H50Q, G51D and A53T) under quiescent conditions at pH 6.5 and 37°C.

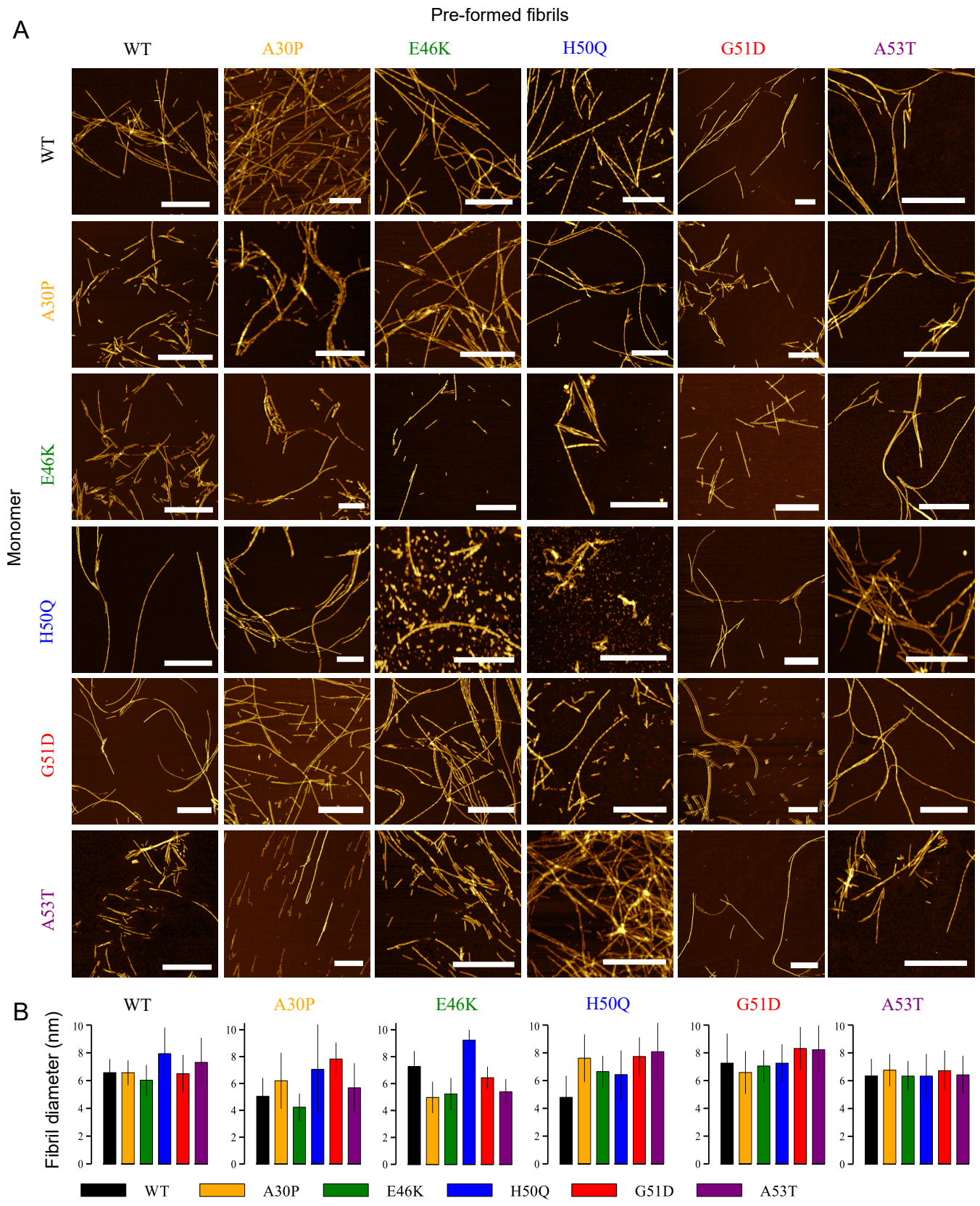

Fig. S5. Fibril morphology of α-synuclein WT and its disease associated mutant variants. (A) AFM images of the fibrils formed by α-synuclein and its disease-associated variants for each monomeric variant aggregating in the presence of pre-formed fibrils from each variant. The scale bars represent 1 μm. (B) Average diameter of the fibrils.

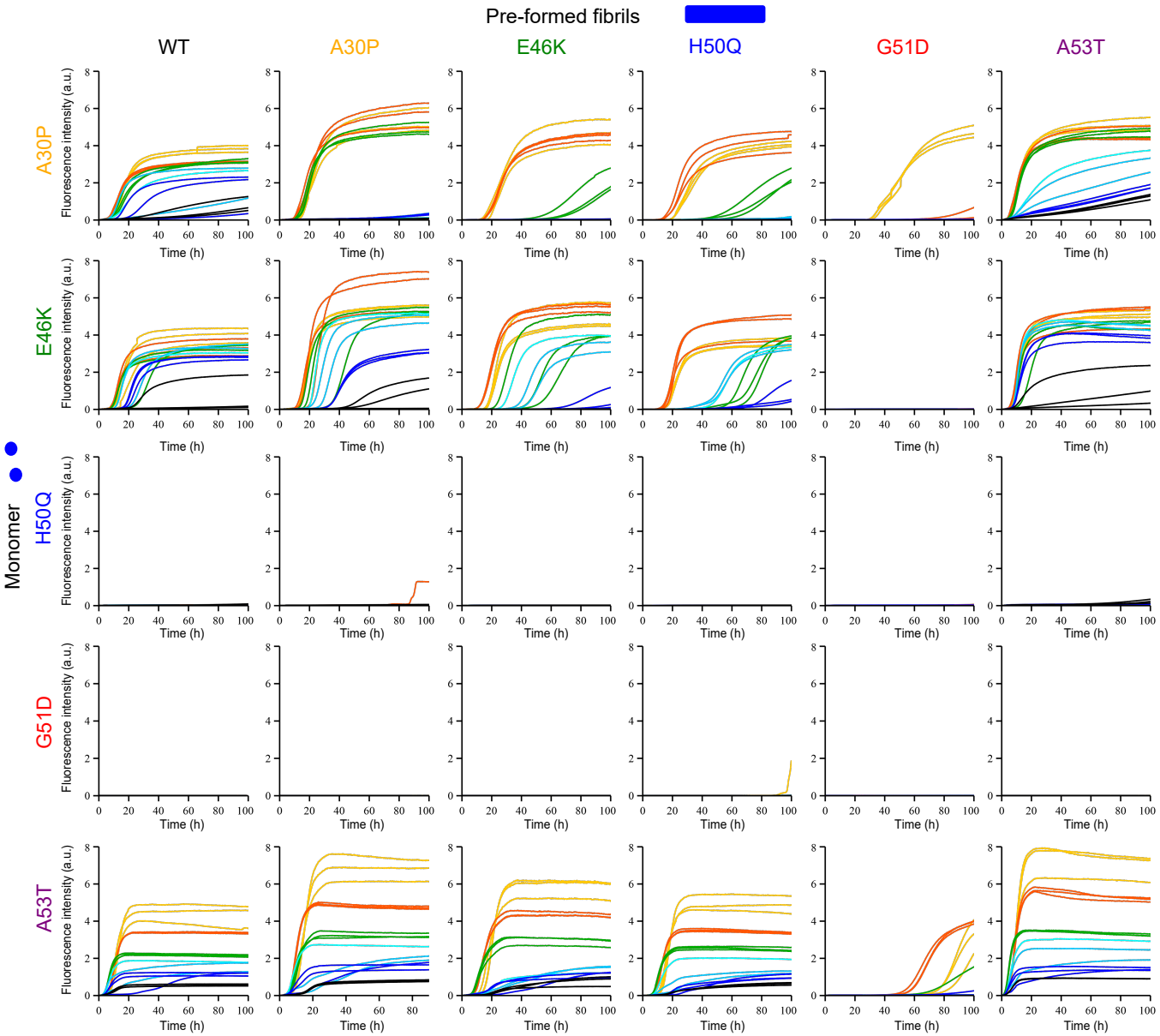

Fig. S6. Fibril amplification at mildly acidic pH of WT α-synuclein and its disease-associated variants. Change in ThT fluorescence intensity when monomeric α-synuclein (WT, A30P, E46K, H50Q, G51D and A53T) was incubated in the presence of 35 nM pre-formed fibrils of the indicated variant (A30P, E46K, H50Q, G51D and A53T) under quiescent conditions at pH 4.8 and 37°C. The protein concentration used in this study were: 20 (black), 30 (dark blue), 40 (light blue), 50 (green), 70 (light green) and 100 μM (yellow).

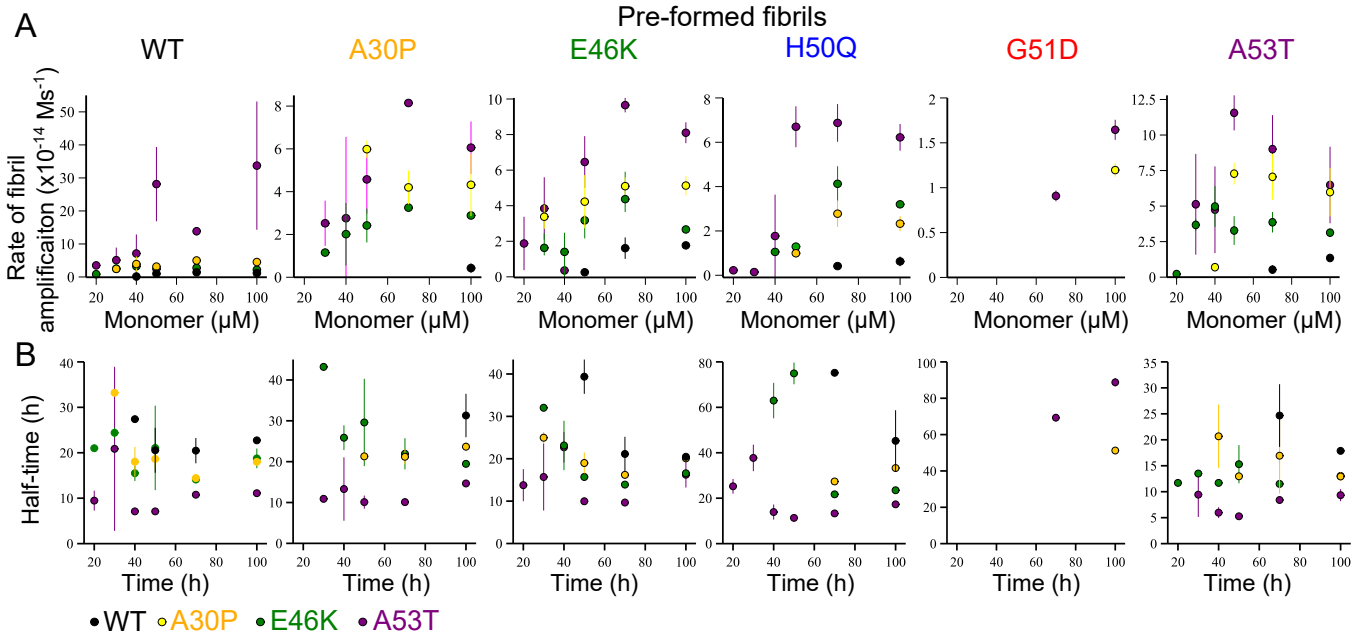

Fig. S7. Fibril amplification at mildly acidic pH of WT α-synuclein and its disease-associated variants. (A) Variation of the rate of fibril amplification of WT (black), A30P (orange), E46K (green), H50Q (blue), G51D (red) and A53T (purple) from WT, A30P, E46K, H50Q, G51D and A53T seeds, respectively, with increasing concentrations of monomeric protein. (B) Half-times of the aggregation experiments.

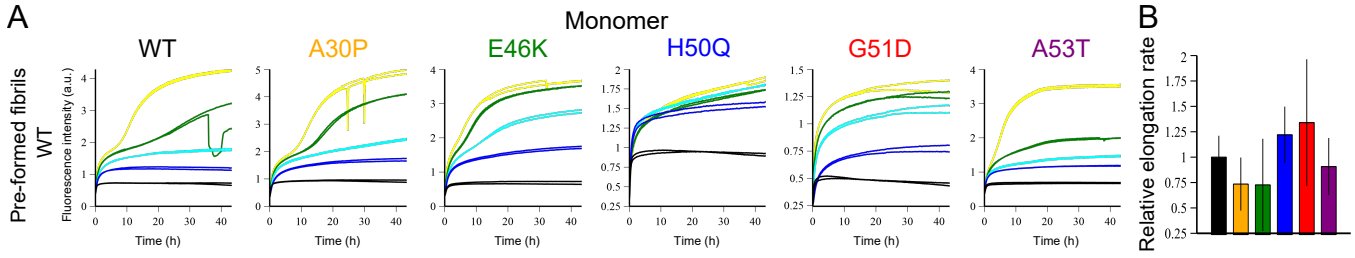

Fig. S8. The elongation rate of α-synuclein is only mildly affected by the disease-associated mutations at acidic pH. (A) Change in ThT fluorescence when monomeric α-synuclein of the indicated mutational variant (WT, A30P, E46K, H50Q, G51D and A53T) at different concentrations (10 (black), 30 (blue), 50 (light blue), 70 (green) and 100 (yellow) μM) was incubated in the presence of 5 μM pre-formed fibrils of the WT protein under quiescent conditions at pH 4.8 and 37°C. (B) Normalized ratios of the elongation rates of the disease-associated variants relative to the rate of the WT protein.

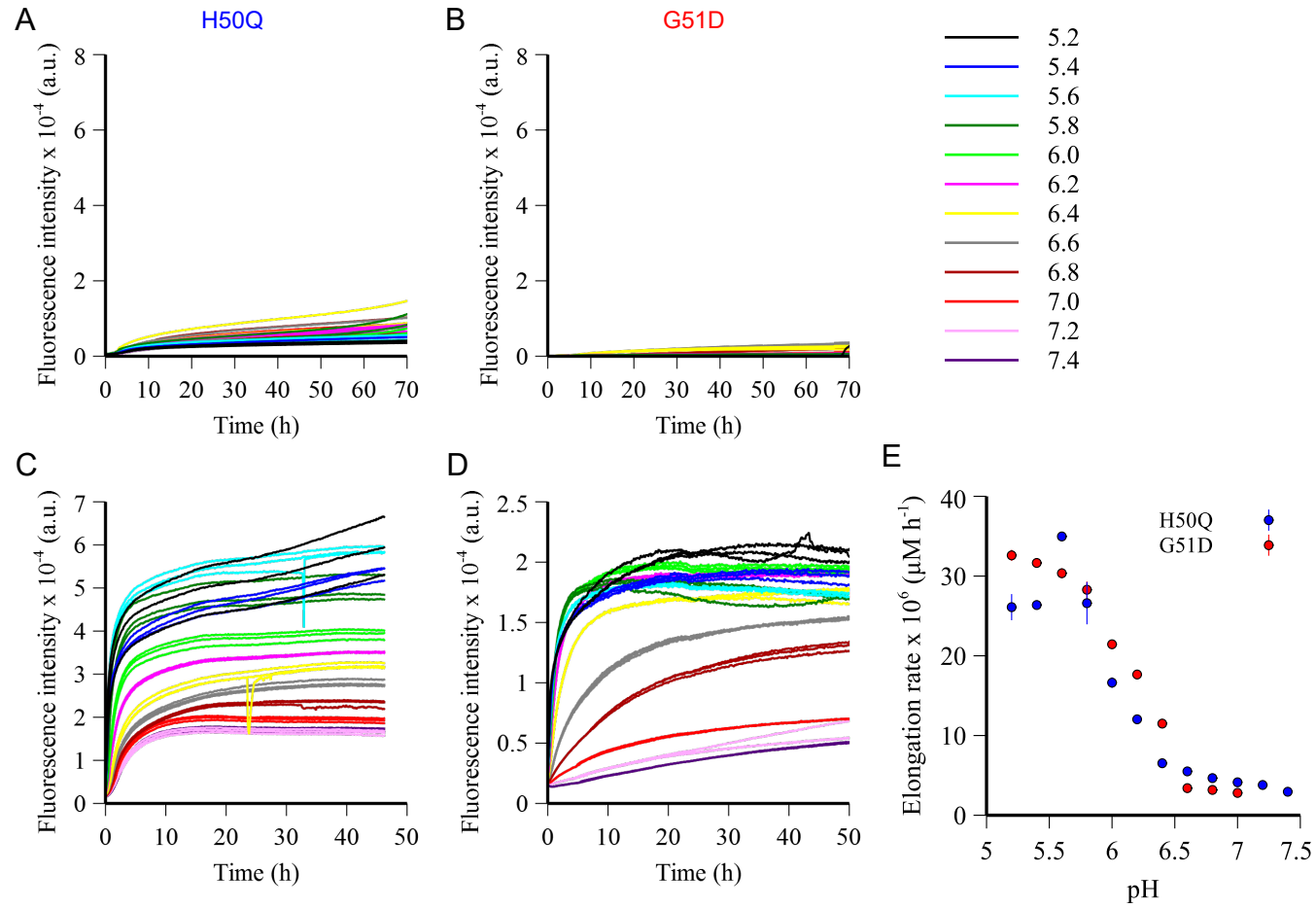

Fig. S9. The pH dependence of fibril amplification and elongation of H50Q and G51D α-synuclein. Change in ThT fluorescence when monomeric H50Q (A) or G51D (B) α-synuclein (50 μM) was incubated in the presence of 35 nM preformed H50Q or G51D seed fibrils, respectively, under quiescent conditions at the pH values indicated and 37°C. Change in ThT fluorescence when monomeric H50Q (C) or G51D (D) α-synuclein (50 μM) was incubated in the presence of 5 μM pre-formed H50Q (C) or G51D (D) seed fibrils under quiescent conditions at the pH values indicated and 37°C. (E) pH dependence of the elongation rate of H50Q (blue) and G51D (red). Rates were determined as described.

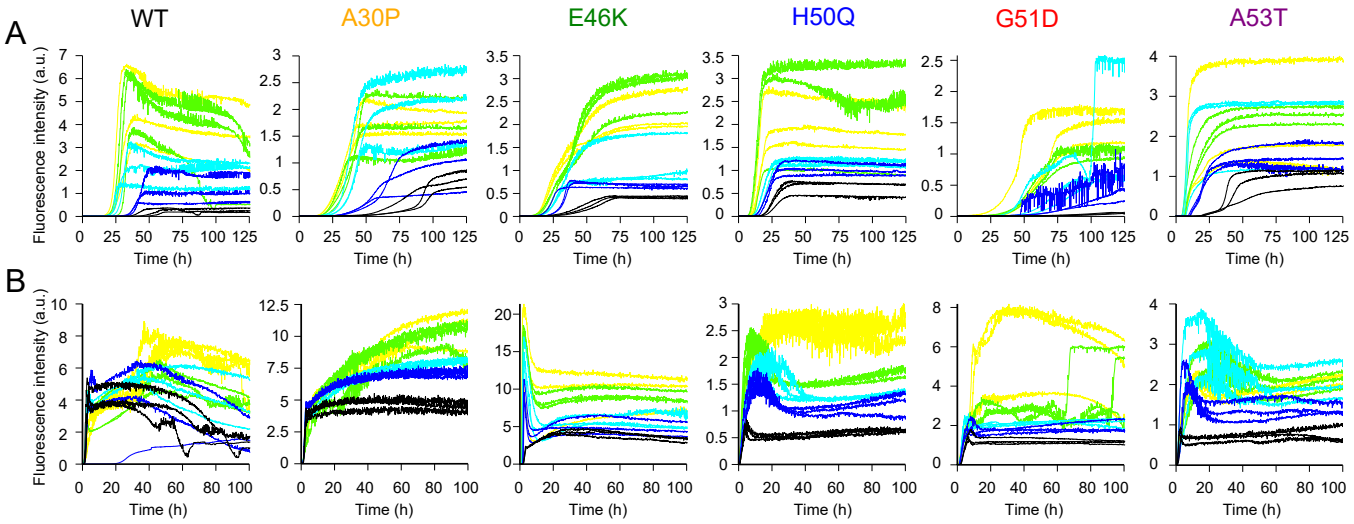

Fig. S10. Aggregation under shaking conditions. Aggregation of WT α-synuclein and its disease associated mutant variants (A30P, E46K, H50Q, G51D, A53T) under shaking conditions at pH 6.5 (A) or pH 4.8 (B), respectively (37°C and 1100 rpm). The ThT fluorescence was measured in aggregation experiments with different monomer concentrations (black: 20 μM, blue: 40 μM, cyan: 60 μM, green: 80 μM, yellow: 100 μM).

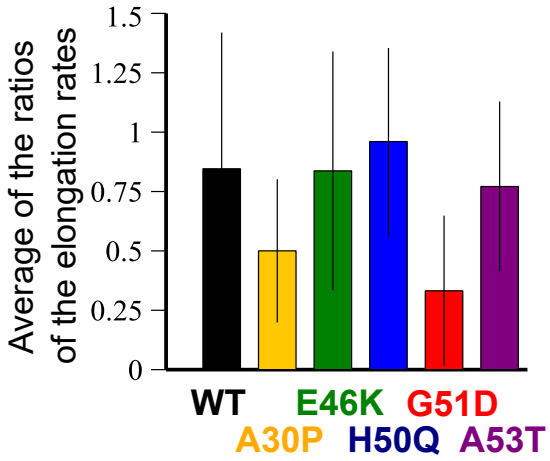

Fig. S11. Mutations associated with Familial Parkinson's disease only mildly affect the elongation step of α-synuclein aggregation. Average of the ratios of elongation rates determined for the elongation of monomeric variants from pre-formed fibrils from all α-synuclein variants studied in this work (data from Fig. 3B).